Journal of Alloys and Compounds 510 (2012) 119–124

Contents lists available at SciVerse ScienceDirect

Journal of Alloys and Compounds

journal homepage: www.elsevier.com/locate/jallcom

SnO_2 dendrites–nanowires for optoelectronic and gas sensing applications

S.H. Mohamed [a,b,*]

[a] Physics Department, College of Science, Qassim University, P.O. 6644, 51452 Buryadh, Saudi Arabia
[b] Physics Department, Faculty of Science, Sohag University, 82524 Sohag, Egypt

ARTICLE INFO

Article history:
Received 5 July 2011
Received in revised form 31 August 2011
Accepted 2 September 2011
Available online 10 September 2011

Keywords:
SnO_2 dendrites–nanowires
FTIR
TGA
Ellipsometer
NO_2 gas sensor

ABSTRACT

SnO_2 dendrites–nanowires were grown on Au coated Si substrates using evaporation condensation method. The morphology, structural, chemical composition and thermal analysis were examined using scanning electron microscopy, X-ray diffraction, energy dispersive analysis of X-ray and Fourier transformation infrared spectroscopy, and thermal gravimetric analysis, respectively. The optical constants, the thickness and the surface roughness of the prepared nanostructured films were determined by spectroscopic ellipsometry measurements. A three layers model was used to fit the calculated data to the experimental ellipsometric spectra. The obtained optical constants were compared with those obtained by other preparation methods. The sensing properties of the obtained SnO_2 nanostructure were carried out for NO_2 gas. The optimal operation temperature was 200 °C and the sensor sensitivity was 40, 56, 83 and 121 for 10, 15, 25 and 50 ppm, respectively.

1. Introduction

Tin oxide (SnO_2) is an n-type semiconductor, which has been extensively studied for various applications, including gas sensors [1–8], catalyst support [9], transparent conducting electrodes [10] and lithium ion battery anode materials [11]. Studies have proven that the properties and performance of SnO_2-based devices can be dramatically influenced by structure features. Therefore, much attention has been paid to the synthesis of one-dimensional (1D) SnO_2 nanostructure like nanowires, nanotubes, nanoribbons, nanobelts, nanorods, etc.

Environmental protection policy of most of the countries is oriented towards the regulation, precise measurement and control of the noxious gases such as H_2S, O_3, CO, H_2 and NO_2 in the atmosphere. Therefore various types of the 1D SnO_2 nanostructure forms have recently gained great prominence as gas sensors [1–4]. For example, SnO_2 nanowires [1,2], SnO_2 nanowires mixed nanodendrites [3], SnO_2 nanofibers [4] have exhibited high nitrogen dioxide (NO_2) and ethanol sensing response.

Air pollution by nitrogen oxides (NO_x), mainly NO and NO_2, is becoming an important environmental issue. As a matter of fact NO_2, associated with other pollutants like volatile organic compounds, is responsible for the formation of ozone in lower atmosphere [12] and smog in urban areas. Also the chemical reaction of NO_2 gas with water vapor causes acid rain [13]. Therefore, the development of NO_2 gas sensor for environmental monitoring has become a necessary task. It is shown that the sensitivity as well as the speed of response to NO_2 largely depends on the synthesis method, nano-additives and the operating temperatures. The monitored gas concentration, response and the operating temperature of doped and undoped SnO_2 sensors for NO_2 gas are currently available in pertinent literatures [1,2,5–8]

The recently proposed evaporation–condensation process, with vapor–solid (VS) and vapor–liquid–solid (VLS) growth mechanisms, which uses SnO_2, SnO and/or Sn as an evaporation source has been successfully used to produce 1D SnO_2 nanostructures [1–3,7]. Thus, in this work, the evaporation–condensation method is used to synthesize SnO_2 nanostructures on Au coated Si substrates. The optical constants are determined by spectroscopic ellipsometer (SE) for optoelectronic applications and the results are compared with results obtained using other preparation methods. The gas sensitivity is evaluated for NO_2 gas.

2. Experimental

The SnO_2 nanostructures were grown using evaporation–condensation method with VLS growth technique. The synthesis processes of SnO_2 were carried out in a controllable horizontal tube furnace with an alumina tube (inner diameter of 44 mm and length of 90 cm). The synthesis was carried out on Au coated (~5–10 nm) Si (1 0 0) wafers (cut into 1 cm × 1 cm and ultrasonically cleaned). The Au coating of Si was done using AC Ion sputtering device (JFC-1100E). The SnO_2 nanostructures were prepared using Sn metal granules, ~3 mm diameter, (Aldrich chemicals; 99.95%). The Sn metal was placed in an alumina boat positioned at the center of the heating zone of the furnace. The Au coated Si substrates were put approximately 1 cm away and a long 10 cm distance from the alumina boat. A mixture of flowing Ar with 300 sccm (standard cubic centimeter per minute) and O_2 with 20 sccm was

* Correspondence address: Physics Department, College of Science, Qassim University, P.O. 6644, 51452 Buryadh, Saudi Arabia. Tel.: +966 0558744839; fax: +966 3800911.
E-mail address: abo_95@yahoo.com

0925-8388/$ – see front matter © 2011 Elsevier B.V. All rights reserved.
doi:10.1016/j.jallcom.2011.09.006

introduced into the alumina tube. Concurrently the temperature was raised rapidly up to 600 °C, and then it was raised with a heating rate of 3 °C/min up to 1050 and kept for 30–60 min. After that, the furnace was cooled down to room temperature.

The surface morphology and crystal structure of the synthesized nanostructures were characterized by scanning electron microscope (SEM) type JOEL model JSM-6380 LA (Japan) and X-ray diffraction (XRD) using Shimadzu Diffractometer XRD 6000, Japan, which utilizing $CuK_{\alpha 1}$ radiation ($\lambda = 1.54056$ Å), respectively. The chemical composition of the synthesized nanostructures was analyzed using energy dispersive analysis of X-ray (EDAX) unit attached with the SEM.

Powder of SnO_2 was scratched easily out of the Au coated Si substrate, grounded and used for Fourier transformation infrared (FTIR) and thermal gravimetric analysis/deferential thermal analysis (TGA/DTA). The SnO_2 powder was mixed with KBr for FTIR measurements. The FTIR measurements were carried out using a Fourier transformation infrared spectrophotometer (IRPrestige-21, SHIMADZU) in the wavenumber range 400–4000 cm^{-1} with 3.85 cm^{-1} resolution and at room temperature (RT). The Shemadzu DTG-60AH Thermo-gravimetric Analyzer enabled simultaneous recording of TGA/DTA. The samples (mass app. 0.814 mg) were heated in a standard platinum pan. The measurements were carried out in air atmosphere. The heating rate was 25 °C/min and started from RT to 1500 °C.

The SE data for SnO_2 nanostructured films were acquired using a PHE-102 variable angle spectroscopic ellipsometer (Angstrom Advanced Inc.) in the wavelength range 350–1100 nm (energy range 3.54–1.13 eV). The data were acquired at angle of incidences of 65° and 70°. The instrument measures the complex ratio of the Fresnel reflection coefficients for p- and s-polarized light and reports the ratio in terms of the ellipsometric parameters ψ and Δ defined by the equation

$$F = \tan(\psi)\exp(i\Delta) = \frac{\tilde{r}_p}{\tilde{r}_s} \quad (1)$$

where $\tilde{r}_p$ and $\tilde{r}_s$ are the amplitude reflection coefficients for light polarized in the p- and s- plane of incidence, respectively. The data obtained from the ellipsometer were accurately modeled using the PHE-102 software package. The ellipsometric ψ and Δ data for variable wavelengths were fitted in the optical model.

In order to make sensors based on the synthesized SnO_2 nanostructures, the method described in Ref. [1] was used. A few drops of ethanol suspended with SnO_2 nanostructures were deposited on a microscopic glass slide and dried at 100 °C to remove the ethanol. Then, a silver electrode was made on the film of the SnO_2 nanostructures by using silver paste and the obtained sensor was connected to an electronic circuit for gas sensing characterization. The area of the sensing element was 1 cm × 1 cm. In order to investigate NO_2 gas sensing properties, the sensors were placed in a quartz tube, which was inserted in an electric furnace. The operating temperature was varied from RT up to 350 °C. The heating rate was 3 °C/min during the change from an operating temperature to the next one. Air, mixed with different concentrations of NO_2 gas, was passed at a rate of 200 ml/min through the quartz tube. The sensor sensitivity was estimated as the ratio of electrical resistances, R_g/R_a, where R_a was the electrical resistance before the introduction of NO_2 gas, and R_g was the maximum electrical resistance after the introduction of NO_2 gas.

3. Results and discussion

3.1. Structural, morphological, compositional and thermal examinations

Fig. 1 shows the XRD pattern of SnO_2 nanostructure. The presence of sharp peaks in this figure indicates that the SnO_2 nanostructure has a polycrystalline nature with high degree of crystallinity. All the diffraction peaks are attributed to various diffraction plans of SnO_2 with tetragonal rutile structure (JCPDS file no. 41-1445). The pattern also confirms that there are no Sn characteristics peaks. The lattice parameters are $a = 4.738$ Å and $c = 3.187$ Å. The mean grain size, calculated from the Scherrer formula [14], is 28 nm. Harris analysis was performed to investigate the preferential orientation of the crystallographic planes in the SnO_2 nanostructure. The texture coefficient $P(h_i\,k_i\,l_i)$, a preferential orientation indicator of the $(h_i\,k_i\,l_i)$ plane, is given by the following equation [15]:

$$P(h_i\ k_i\,l_i) = \left(\frac{I(h_i\,k_i\,l_i)}{I_r(h_i\,k_i\,l_i)}\right)\left(\frac{1}{m}\sum_{i=1}^{m}\frac{I(h_i\,k_i\,l_i)}{I_r(h_i\,k_i\,l_i)}\right)^{-1} \quad (2)$$

where $I(h_i\,k_i\,l_i)$ is the diffraction intensity of the $(h_i\,k_i\,l_i)$ plane of the sample under investigation, $I_r(h_i\,k_i\,l_i)$ is the intensity of the $(h_i\,k_i\,l_i)$ plane of a random powder sample and m is the number of diffraction peaks. Eq. (2) shows that $P(h_i\,k_i\,l_i)$ of each crystallographic plane is unity for a randomly distributed powder sample,

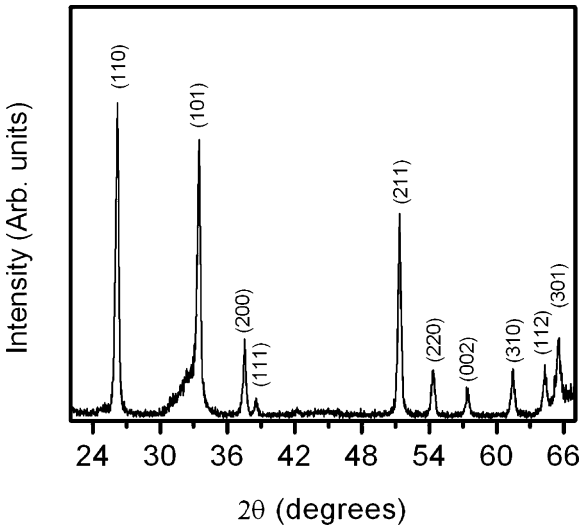

Fig. 1. XRD pattern of the synthesized SnO_2 nanostructure.

whereas is larger than unity if $(h_i\,k_i\,l_i)$ plane is preferentially oriented. The Harris analysis results are summarized in Table 1. The texture coefficient value of the index (1 1 1) plane is the highest indicating that is more preferentially oriented.

Typical SEM images presenting morphologies of the synthesized SnO_2 on Au coated Si substrates are shown in Fig. 2a and b, with lower and higher magnifications, respectively. It revealed that the white SnO_2 products are nanowires with fuzzed branches. The nanowires are distributed randomly on the Au coated Si substrate. This morphology has been obtained previously on Au coated alumina [3]. The fuzzy branches can be called nanodendrites, which are meandering chains with random branches [3]. The lengths of the nanodendrites are in the range 72–97 nm, which are the same as the diameters of the nanowires. The lengths of the nanowires are in the range of 3–9 μm. A possible explanation of the formation of the SnO_2 dendrites–nanowires (DNWs) is as follows. The melted Au catalyst forms a liquid droplet and the Sn atoms or SnO_2 molecules stick to it and thereby forms a dendrite via VLS growth mechanism. The newly arriving vaporized precursor may precipitate on the dendrite and form a new dendrite. This process is regularly repeated and hence forms dendrites–nanowires.

VLS and VS growth mechanisms are well accepted as growth mechanisms of SnO_2 1D nanostructures [1–3]. It is generally known that the growth process of 1D nanostructure is dominated by kinetics rather than thermodynamics. Nanoscale 1D structures of oxides prepared by thermal evaporation can be grown in either VLS or VS mechanism depending on the kind of material and the process condition [16]. The VLS mechanism is generally dominated in the thermal evaporation process carried out with the aid of a metal

Table 1
X-ray diffraction intensities and preferred orientation factors of SnO_2 dendrites–nanowires.

$(h\,k\,l)$	I	I_r[a]	P_{hkl}
(1 1 0)	537	100	0.73
(1 0 1)	477	75	0.86
(2 0 0)	135	21	0.89
(1 1 1)	40	4	1.35
(2 1 1)	349	57	0.83
(2 2 0)	84	14	0.81
(0 0 2)	54	6	1.22
(3 1 0)	84	11	1.0
(1 1 2)	89	12	1.0
(3 0 1)	135	14	1.30

[a] From JCPDS, International Centre for Diffraction Data, 1996.

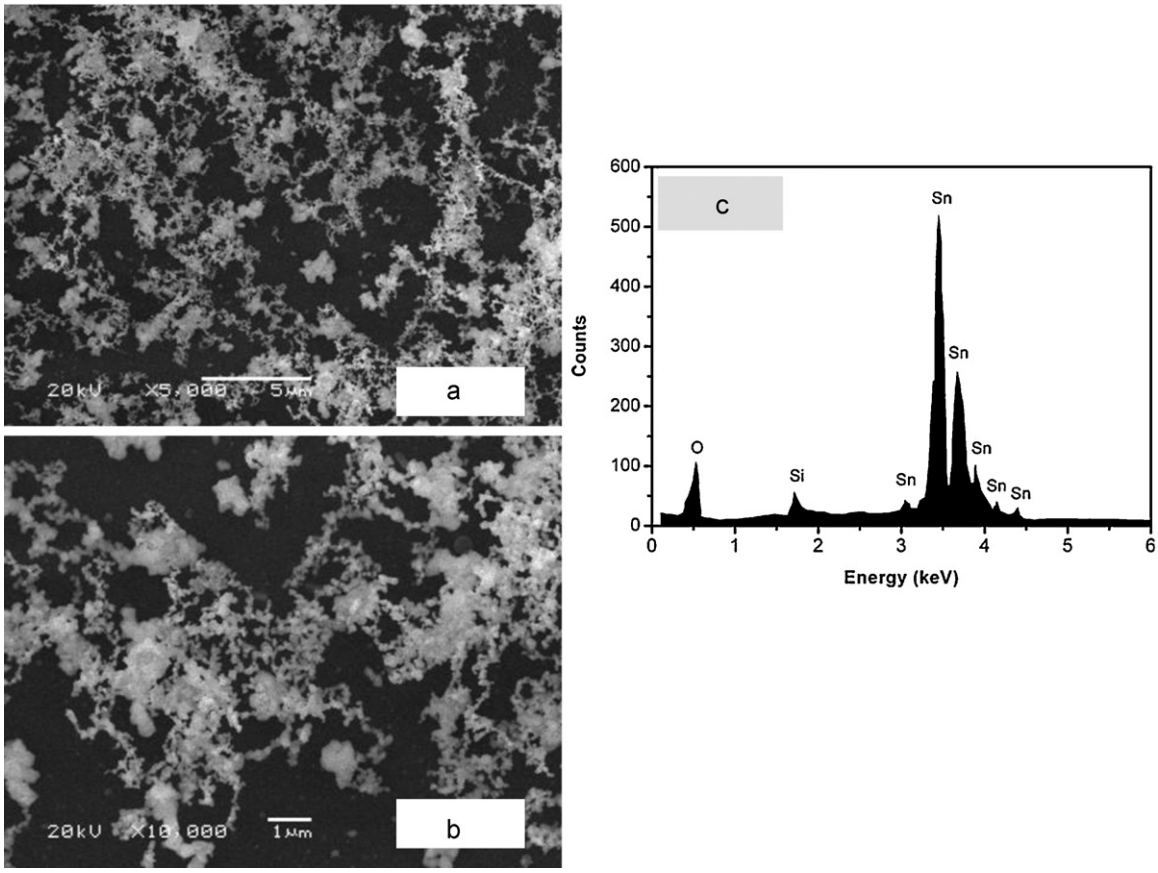

Fig. 2. Low and high magnifications SEM images (a and b) and EDAX spectrum (c) of SnO_2 DNWs.

catalyst (Au in our case). Nevertheless, the absence of catalyst particles at the end of nanowires does not necessarily mean that the growth of the nanowires is governed by a VS process, especially for the oxide nanostructures. This is because, in some cases, the metal catalyst, which affects the reaction condition, may be oxidized into the oxide tip with the same composition as the nanowires during cooling the furnace to room temperature [16].

The chemical composition of the as-synthesized SnO_2 nanostructure, characterized by EDAX, is shown in Fig. 2c. It is found that the nanostructure is manly composed of Sn and O together with a small peak marked Si. The Si peak is steamed from the Si substrate. The atomic percents of Sn and O elements are $(31.28 \pm 2)\%$ and $(63.72 \pm 2)\%$, respectively. For the EDAX measurement, different positions of SnO_2 nanostructure show almost the same ratio of O/Sn. The results show that the DNWs are composed of O and Sn with the ratio of O/Sn slightly higher than 2. This suggests that the prepared product is SnO_2 with little excess of oxygen.

FTIR provides the most direct information about the local bonding of constituent atoms and hence about local molecular structure of the film. The FTIR absorbance spectrum of SnO_2 DNWs is drawn in Fig. 3. The absorption peaks of 3688 cm^{-1}, 1300 cm^{-1}, 1053 cm^{-1} and 918 cm^{-1} are suggesting that there are some O–H bonds on the SnO_2 DNWs [17] which are assigned to the vibrations of different types of surface hydroxyl groups. Additionally, the band at 1525 cm^{-1} may be assigned to C–H vibrations or to the vibration harmonics of Sn–O–Sn bridges obtained by condensation of hydroxyl groups [17]. According to the literature [18], the C–H may result from the adsorption and interaction of atmospheric carbon dioxide with water. The Sn–O and Sn–O–Sn vibrations appeared in the range of 400–700 cm^{-1} as the result of condensation reaction [17,19]. The peaks at 674 and 636 cm^{-1} are attributed to the Sn–O–Sn antisymmetric vibrations and the peaks at 558 and 520 cm^{-1} are attributed to the Sn–O stretching vibrations.

The simultaneously recorded TGA and DTA thermogram, performed on powder of SnO_2 DNWs scratched out of the Au coated Si substrates, is shown in Fig. 4a and b, respectively. It is clear from Fig. 4a that the adsorbed water and gases in the sample and the crucible are removed below 500 °C. The weight loss increases gradually with increasing temperature up to a certain temperature (~1100 °C) beyond which a sharp weight gain is started. This sharp

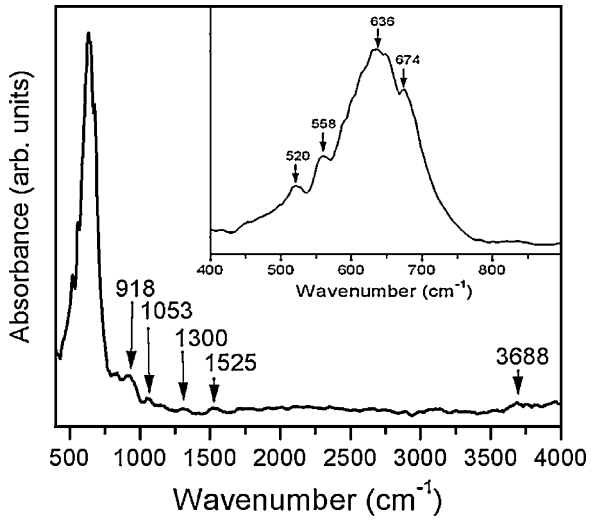

Fig. 3. FTIR absorbance spectrum of SnO_2 DNWs.

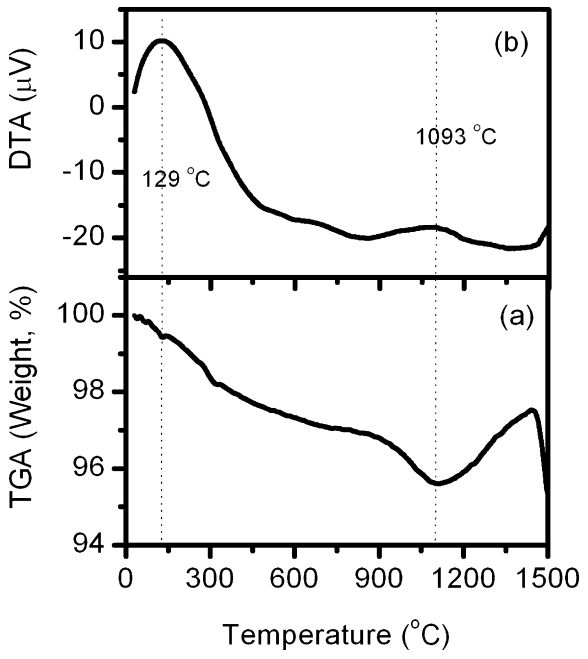

Fig. 4. TGA (a) and DTA (b) thermogram of SnO_2 DNWs.

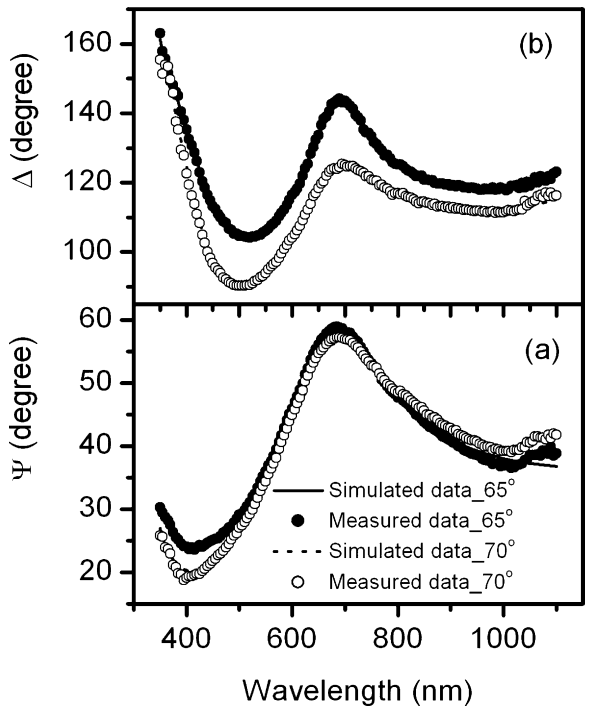

Fig. 5. Measured and calculated ψ and Δ spectra at 65° and 70° angles of incidence for of SnO_2 DNWs film.

increase in weight may be attributed to the oxidation of some possibly present, in the interstitial positions of the oxide, Sn metal atoms [20]. It is worth mentioning that there are two broad exothermic peaks in the DTA curve (Fig. 4b) corresponding to the main mass losses positions at the TGA curve.

Based on the appearance O–H absorption bands, in the FTIR spectrum, and the weight loss (the net weight loss at 1100 °C is 4.4% of the original weight), observed at the DTA curve, it can be concluded that some of the oxygen revealed by EDAX are not chemically bonded with Sn but it is adsorbed on the surface of the SnO_2 DNWs and the obtained SnO_2 DNWs are slightly beyond the stoichiometric SnO_2.

3.2. Ellipsometric study of the prepared SnO_2 nanostructure films

3.2.1. Ellipsometric modulation

The choice of the appropriate optical model plays a major role in the evaluation of the optical constants from the SE spectra. Thus, the refractive index (n) and extinction coefficient (k) of SnO_2 nanostructured films were obtained by assuming a three-layer model, representing the interface layer, the film and the surface roughness layer. The interface layer was modeled using published optical constants of Au, which installed in the software package and the complex refractive index of the film was described by the Cauchy dispersion relation. The complex refractive index of the surface roughness layer was calculated by the BEMA assuming a mixture of the "Lorentz oscillator – material" and a fitted percentage (volume fraction) of voids (air). The Cauch–Urbach dispersion relation can be expressed as:

$$n(\lambda) = A_n + \frac{B_n}{\lambda^2} + \frac{C_n}{\lambda^4}, \qquad k(\lambda) = \alpha' \exp\left(\beta\left(\frac{1}{\lambda} - \frac{1}{\lambda_0}\right)\right) \tag{3}$$

The six parameters in this dispersion model are A_n, B_n, C_n, the extinction coefficient amplitude α', the exponent factor β, and the wavelength corresponding to the band gap value λ_0. All the Cauch–Urbach six parameters, the thickness and the voids fraction of the BEMA surface layer and the thickness of the interface layer were used as a variable fit parameter.

An example for the best fit of the proposed model compared with the measured ellipsometric data of SnO_2 DNWs films at 65° and 70° angles of incidences is shown in Fig. 5a and b. It is seen that there is a good agreement between the simulated and the measured data. Thus the optical constants can be adequately extracted. The thickness (interfacial/film/surface), Cauchy's coefficients (A_n, B_n and C_n), Urbach's coefficients (α', β, λ_0), the voids fraction and the mean square error (MSE) determined by VASE data fits are summarized in Table 2.

3.2.2. Optical constants of SnO_2 dendrites–nanowires

Fig. 6 shows the refractive index (n) and the extinction coefficient (k) at the measuring wavelength from 350 to 1100 nm of the SnO_2 DNWs film. One can see that the refractive index first increases with the wavelength up to 404 nm and then decreases

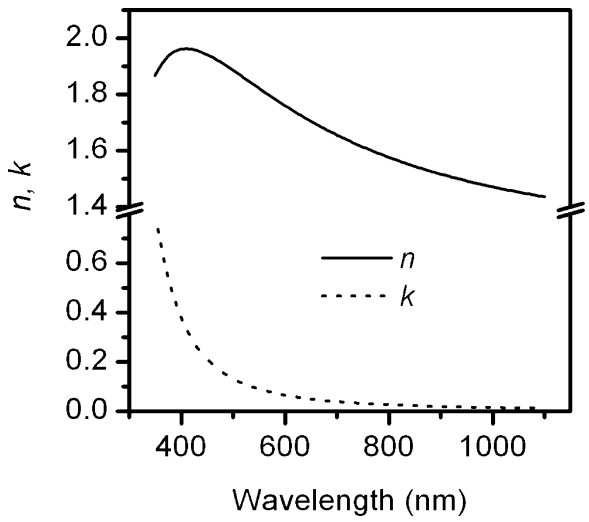

Fig. 6. The refractive index (a) and extinction coefficient (b) of SnO_2 DNWs film.

Table 2
Thickness derived from the elliposmetric data fitting (interfacial/film/surface roughness), Cauchy's coefficients (A_n, B_n and C_n), Urbach's coefficients, voids fraction and the mean square error (MSE).

Thickness (nm) (interfacial/film/surface roughness)	Cauchy's coefficients			Urbach's coefficients			Voids fraction (%)	MSE
	A_n	B_n (nm^2)	C_n (nm^4)	α'	β	λ_0 (nm)		
8.2/166.3/9.4	1.397	0.1243	−0.0215	0.01459	1.1308	410	55.23	3.96

normally with wavelength. The variation of refractive index is similar to that of polycrystalline textured SnO_2:F films prepared on glass substrates by using low-pressure chemical-vapor deposition [21] and on p-InSb (1 1 1) substrates by using radio-frequency magnetron sputtering [22]. It is also interesting that mentioning the magnitude of n at $\lambda = 420$ nm is, 1.96, very close to the bulk value of SnO_2 (i.e. $n = 2$) [23]. This confirms the high optical quality of the SnO_2 thin films prepared by the used method. The k values of the SnO_2 DNWs decrease with increasing wavelength and became much closer to zero at higher wavelengths.

The absorption coefficient (α) was calculated using the obtained k values from the relation:

$$\alpha = \frac{4\pi k}{\lambda} \tag{4}$$

For crystalline SnO_2, optical transitions have been shown to be direct [24]. The variation in the absorption coefficient as a function of photon energy for allowed direct transitions is given by

$$(\alpha h\nu) = A(h\nu - E_g)^{1/2} \tag{5}$$

where A is a constant, h is Planck's constant, ν is the frequency, and E_g is the band gap energy. The E_g value is obtained by extrapolating the linear part to intercept with the energy axis (Fig. 7a) and is found to be 3.20 ± 0.02 eV. This value is very close to the value 3.22 eV obtained for SnO_2 grown by spray deposition [25]; however, it is lower than the recently reported values 3.95 eV [26] and 4.15–4.30 eV [27] for SnO_2 grown by ultrasonic spray pyrolysis and RF-magnetron sputtering techniques, respectively. The low value may be ascribed to the slight deviation from stoichiometric SnO_2 as revealed by TGA analysis.

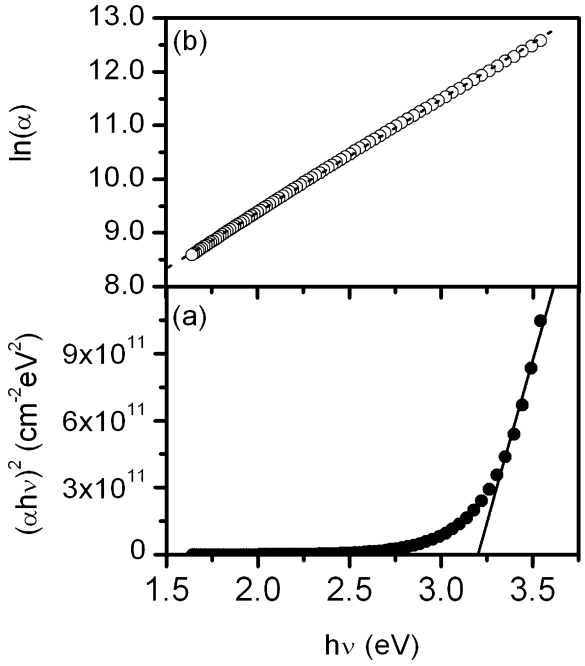

Fig. 7. (a) Plot of $(\alpha h\nu)^2$ versus $h\nu$, and (b) $\ln(\alpha)$ versus $h\nu$.

To evaluate the near band gap edge characteristics of the SnO_2 DNWs, the absorption behavior at lower photon energy can be interpreted by the Urbach rule:

$$\alpha = K \exp(E/E_u) \tag{6}$$

where K is constant and E_u is Urbach energy which is interpreted as the width of the tails of localized states in the band gap [28]. The absorption in this region is due to transitions between extended states in one band and localized states in the exponential tail of the other band as well as the effects of all defects [29]. Plotting $\ln\alpha$ as a function of energy, as shown in Fig. 7b, the E_u can be calculated. The obtained E_u value is 474 meV. The obtained E_u value for the SnO_2 DNWs is higher than the reported value, 270 meV, for the ultrasonic spray pyrolysis deposited SnO_2 [26], however, it lies among the values 386–789 meV reported for RF-magnetron sputtering [27]. It suggests that the defects in the SnO_2 depend mainly on the preparation conditions used in the CVD or the PVD method and not on the method itself.

3.3. SnO_2 DNWs sensing properties

The SnO_2 DNWs sensor sensitivity as function of operating temperatures is shown in Fig. 8. The sensitivity of the sensor increases with temperature and reaches the optimal temperature at about 200 °C. The highest sensor sensitivities for 10, 15, 25 and 50 ppm of NO_2 concentrations are 40, 56, 83 and 121, respectively. The response time is defined as the time to reach 90% of the $(R_g–R_a)$ value was found, at the optimal temperature 200 °C, to be 39, 27, 15 and 6 s for 10, 15, 25 and 50 ppm of NO_2 concentrations, respectively. The sensor sensitivity in this work is comparable to that of the SnO_2 nanowires [2] and the SnO_2 nanoparticles [30].

The sensing mechanism of resistive solid state gas sensors mainly relies on the change of electrical resistivity (or conductivity) resulting from the interactions between sensors surface and the target gases [31]. When SnO_2 is exposed to the oxidizing gas such as NO_2, oxygen molecules are adsorbed on the surface. The

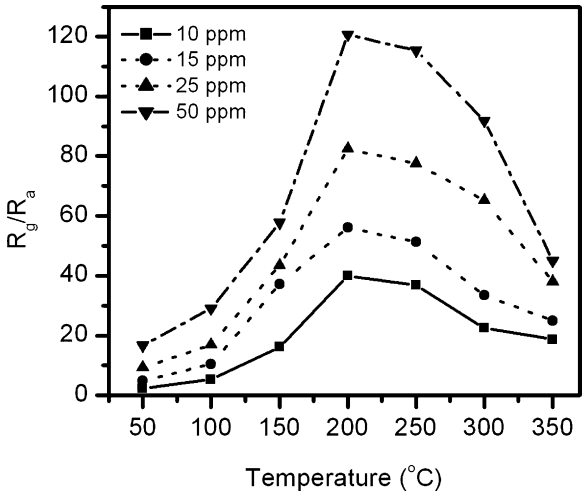

Fig. 8. The SnO_2 DNWs sensor sensitivity versus operating temperature under NO_2 concentrations of 10, 15, 25 and 50 ppm.

adsorbed oxygen molecules extract electrons from SnO_2, thereby, forming oxygen ions (O^- and/or O^{2-}) on the surface. The extraction of electrons makes a depletion region on the nanostructure surface that leads to the increase in the resistance.

At low operating temperatures (below 200 °C), the result of the reaction between the adsorbed target gas (NO_2) and the resident oxygen (RO) in the surface of the sensor could not be separated from the sensor's surface. Therefore, reaction between the target gas and the sensor's surface could not be easily proceed because of the aggregation of RO at the surface of the sensor, and as a result the sensitivity of the sensor is low at lower temperatures [4]. The elevation of the temperature facilitates the separation of RO from the sensor's surface and could facilitate the reaction between the target gas and the sensor's surface. Furthermore, the rate of reducing reaction increases with the increase of temperature, which causes an increase of the sensitivity of the sensor. The rate of adsorption of reducing gas at the sensor's surface decreases with further increase of temperature and therefore, causes a decrease of sensitivity due to the decreases of the reducing reaction.

4. Conclusion

Mixed morphology of SnO_2 nanodendrites and nanowires was successfully synthesized by the evaporation condensation method. The XRD and EDAX analysis revealed the presence of single crystalline phase of tetragonal rutile structure with stoichiometric composition. However, the analysis of FTIR and TGA indicated the possibility of substoichiometric; as some oxygen was adsorbed on the nanostructure surface. The thickness and optical constants were accurately determined from the SE, which may prove useful in the design of nano-optoelectronic devices. The fabricated nanostructure SnO_2 sensors showed high sensitivity and quick response at the optimal operation temperature.

Acknowledgments

This work is supported by the Long-Term Comprehensive National Plan for Science, Technology and Innovation General Secretariat under contract no. 09-ENV791-09, and in cooperation with the Deanship of Scientific Research at Qassim University & KACST. Mr. Ahmed S. Radwan, at chemistry department, is acknowledged for his technical support.

References

[1] N.M. Shaalan, T. Yamazaki, T. Kikuta, Mater. Chem. Phys. 127 (2011) 143.
[2] B.-G. Kim, D.-G. Lim, J.-H. Park, Y.-J. Choi, J.-G. Park, Appl. Surf. Sci. 257 (2011) 4715.
[3] S. Phadungdhitidhada, S. Thanasanvorakun, P. Mangkorntong, S. Choopun, N. Mangkorntong, D. Wongratanaphisan, Curr. Appl. Phys. 11 (2011) 1368.
[4] H.A. Khorami, M. Keyanpour-Rad, M.R. Vaezi, Appl. Surf. Sci. 257 (2011) 7988.
[5] S.-W. Choi, S.-H. Jung, S.S. Kim, Significant enhancement of the NO_2 sensing capability in networked SnO_2 nanowires by Au nanoparticles synthesized via γ-ray radiolysis, J. Hazard. Mater., in press.
[6] I.-S. Hwang, S.-J. Kim, J.-K. Choi, J. Choi, H. Ji, G.-T. Kim, G. Cao, J.-H. Lee, Sens. Actuators B 148 (2010) 595.
[7] N.M. Shaalan, T. Yamazaki, T. Kikuta, Sens. Actuators B 153 (2011) 11.
[8] H.S. Kim, S.E. Park, H.W. Kim, J.Y. Park, N. Jiang, S.S. Kim, Solid State Sci. 12 (2010) 970.
[9] N. Kakati, J. Maiti, S.H. Jee, S.H. Lee, Y.S. Yoon, J. Alloys Compd. 509 (2011) 5617.
[10] E. Chan, Díaz, M. Juan, A. Camacho, R. Duarte-Moller, P. Castro-Rodríguez, Bartolo-Pérez, J. Alloys Compd. 508 (2010) 342.
[11] F. Wang, G. Yao, M. Xu, M. Zhao, Z. Sun, X. Song, J. Alloys Compd. 509 (2011) 5969.
[12] B.T. Marquis, J.F. Vetelino, Sens. Actuators B 77 (2001) 100.
[13] J. Brunet, V.P. Gracia, A. Pauly, C. Varenne, B. Lauron, Sens. Actuators B 134 (2008) 632.
[14] B.D. Cullity, Elements of X-Ray Diffraction, 2nd ed., Addison-Wesley, Reading, MA, 1979, p. 102.
[15] C.S. Barrett, T.B. Massalski, Structures of Metals, Pergamon, Oxford, 1980, p. 204.
[16] S. Park, C. Hong, J. Kang, N. Cho, C. Lee, Curr. Appl. Phys. 9 (2009) S230.
[17] D. Amalric-Popescu, F. Bozon-Verduraz, Catal. Today 70 (2001) 139.
[18] S. Emiroglu, N. Barsan, U. Weimar, V. Hoffmann, Thin Solid Films 391 (2001) 176.4.
[19] Z. Li, W. Shen, X. Zhang, L. Fang, X. Zu, Colloids Surf. A 327 (2008) 17.
[20] S.H. Mohamed, Philos. Mag. 91 (2011) 3598.
[21] P.I. Rovira, R.W. Collins, J. Appl. Phys. 85 (1999) 2015.
[22] T.W. Kim, D.U. Lee, D.C. Choo, J.H. Kim, H.J. Kim, J.H. Jeong, M. Jung, J.H. Bahang, H.L. Park, Y.S. Yoon, J.Y. Kim, J. Phys. Chem. Solids 63 (2002) 881.
[23] V.M. Jimenez, J.P. Espinos, A. Caballero, L. Contreras, A. Fernandez, A. Justo, A.R. Gonzalez-Elipe, Thin Solid Films 353 (1999) 113.
[24] J. Robertson, J. Phys. Chem. 12 (1979) 4767.
[25] H. Demiryont, K.E. Nietering, Sol. Energ. Mater. 19 (1989) 79.
[26] F. Atay, V. Bilgin, I. Akyuz, E. Ketenci, S. Kose, J. Non-Cryst. Solids 356 (2010) 2192.
[27] S. Saipriya, M. Sultan, R. Singh, Physica B 406 (2011) 812.
[28] J.C. Tauc, Optical Properties of Solids, North-Holland, Amsterdam, 1972; J.C. Tauc, Amorphous and Liquid Semiconductors, Plenum Press, New York, 1974.
[29] V. Srikant, D.R. Clarke, J. Appl. Phys. 81 (1997) 6357.
[30] A. Sharma, M. Tomar, V. Gupta, Sens. Actuators B 156 (2011) 743.
[31] J. Huang, Q. Wan, Sensors 9 (2009) 9903.